ARTICLE

Aminoclay: A Designer Filler for the Synthesis of Highly Ductile Polymer-Nanocomposite Film

G. Johnsy,[†] K. K. R. Datta,[‡] V. A. Sajeevkumar,[†] S. N. Sabapathy,[†] A. S. Bawa,[†] and M. Eswaramoorthy*,[‡]

Food Engineering and Packaging Division, Defence Food Research Laboratory, Siddarthanagar, Mysore, India 570 011, Nanomaterials and Catalysis Lab, Chemistry and Physics of Materials Unit and DST Unit on Nanoscience, Jawaharlal Nehru Centre for Advanced Scientific Research, Jakkur, Bangalore, India 560 064

ABSTRACT Water-dispersible aminoclay synthesized in a single step process was used as an inorganic filler for preparing polyvinyl alcohol (PVA)−clay hybrid films. The PVA−clay hybrid films with different weight percentages of aminoclay were obtained by simple mixing and casting of aqueous solutions of clay and polymer. The composite films show excellent retention of ductile behavior of the polymer, PVA, even at higher loadings (20 wt %) of aminoclay. Introduction of aminoclay stabilized Ag nanoparticles significantly improved the mechanical properties of the composite film. The oxygen barrier property of the composite film was improved with the increase in composition of the clay.

KEYWORDS: polyvinyl alcohol (PVA) • aminoclay • polymer−clay nanocomposites films • Ag nanoparticles • hybrid films.

INTRODUCTION

Nanoparticle-incorporated polymer matrices are known to show properties significantly different from the parent polymer because of the complex enthalpic and entropic interactions (1, 2). Among the different polymer−nanoparticles composites, polymer−clay nanocomposites have generated a great deal of interest in materials science because of their improved mechanical properties, enhanced ionic conductivity, reduced gas permeability and thermal expansion in comparison to the pure polymer or polymer−clay microcomposites (3−8). The great challenge in obtaining these properties, however, lies in the homogeneous mixing of clay nanoplatelets within the polymer matrix. Direct blending to obtain polymer−clay nanocomposites often suffers with inhomogeneous mixing, especially with the commercial clays because of their poor miscibility and incomplete exfoliation within the polymer matrix (9). The poor miscibility of inorganic clays in water also limits their uniform mixing with water-soluble polymers such as polyvinyl alcohol (10) (PVA) and polyethylene oxide (11) (PEO) beyond a certain composition. Another major drawback in using commercial clays as fillers is the drastic reduction of plastic yielding of the resulting composite at higher loading (leading to a catastrophic rupture) while improving its strength. In addition, these clays often require post-modification with long-chain surfactants before being used as inorganic fillers to modify the strength of the resulting polymer−clay composites. Nevertheless, several polymer nanocomposites consisting of organically modified (both by intercalation and exfoliation) montmorillonite, hectorite, and smectite clays and water-soluble polymers have been reported by solution-intercalation film-casting method (12). Because the properties of these nanocomposites depend on the extent of dispersion of clays, which in turn depends on the degree of exfoliation achieved during the process, it is paramount to design new and simple methods to exfoliate clays to a maximum extent. One such method is to synthesize tailor made clays like layered magnesium organosilicates, which can be easily exfoliated in water or oil suiting to the nature of polymer used to make the nanocomposites. Layered magnesium organosilicates are phyllosilicate clays with the structures analogous to 2:1 trioctahedral smectites, such as talc but with covalently linked organosilicates in place of inorganic silicates, with an approximate composition $R_8Si_8Mg_6O_{16}$ $(OH)_4$ where R = alkyl or alkylamine (13). By tailoring the organic functional groups attached to the Mg phyllosilicate networks, we can make these clays as either hydrophobic or hydrophilic (14, 15) suitable for a particular polymer. For example, by introducing amino pendants in the silicate network, the clay can be made completely water-dispersible.

Polyvinyl alcohol, a commercially important water-soluble polymer (16), can form transparent films on drying the PVA solution. The high efficiency to form hydrogen bonds and its superior ability to transfer load between the polymer and inorganic clay layers make this polymer a better candidate for the production of stronger polymer−clay nanocomposites (17, 18). In this study, we have reported a simple and straightforward route to synthesize a polymer−clay nanocomposite exhibiting high retention of optical trans-

* Corresponding author. E-mail: eswar@jncasr.ac.in.
Received for review August 11, 2009 and accepted November 9, 2009
[†] Defence Food Research Laboratory.
[‡] Jawaharlal Nehru Centre for Advanced Scientific Research.
DOI: 10.1021/am9005226

Published on Web 11/24/2009

parency and plasticity even at higher loading (of clay) using a tailor made amine functionalized clay as the filler and the water-soluble PVA polymer as the host. The use of aminoclay as the filler served three purposes. First, the protonation of amino groups within the layers upon addition of water makes the clay layers to exfoliate completely (even at very high concentration) by repulsion and thus impart more miscibility when used along with water-soluble polymers like PVA. Second, the presence of covalently attached organic moieties within the clay platelets gives more flexibility (19) to the otherwise hard inorganic filler and therefore, improves the plasticity of the resulting nanocomposites. Thirdly, these aminoclay nanosheets can strongly stabilize the metal nanoparticles which can be utilized in synthesizing antimicrobial PVA nanocomposites containing Ag nanoparticles. We have also shown here the synergistic effects of metal nanoparticles like Ag and Au in improving the strength of these nanocomposites. Nanosilver is well-known for its antimicrobial properties (20) and thus our aim was to integrate various properties like enhanced mechanical strength, high gas-barrier properties, and antimicrobial activity in a single polymer film without compromising its flexibility.

EXPERIMENTAL SECTION

Synthesis of Aminoclay and Aminoclay Stabilized Nanoparticles. Amine functionalized nanoclay was prepared at room temperature by using an organosilane precursor like 3-aminopropyltriethoxysilane (1.3 mL, 5.85 mmol) as reported earlier (21). This precursor was added drop wise to a solution of magnesium chloride (0.84 g, 3.62 mmol) in ethanol (20 g) under constant stirring at room temperature for 24 h. White gel type material obtained after reaction was recovered by centrifugation followed by washing with ethanol and distilled water and dried at 313 K. Further the amine terminated clays were used for capping metal nanoparticles like Ag and Au by using $AgNO_3$ and $HAuCl_4$ metal precursors. In the case of Ag nanoparticles, aminoclay was prepared using $Mg(NO_3)_2$ as the magnesium source to avoid precipitation of AgCl. Aminoclay was first exfoliated by dispersing 20 mg of clay in 2 mL of millipore water by sonication for 2 min. To this transparent clay suspension, 2 mL of 1 mM metal precursor solution was added followed by the addition of 2 ml of 0.1 mol/L $NaBH_4$ solution. The metal (Ag and Au) loading with respect to aminoclay was maintained at 1 wt %. Immediately, the color of the solution turned to bright yellow and pink, showing the formation of Ag and Au nanoparticles, respectively. A flowchart depicting the synthesis of aminoclay, aminoclay stabilized nanoparticles and PVA–aminoclay nanocomposite films are given in Scheme 1.

Casting of PVA–Aminoclay Nanocomposite Films. PVA solution was prepared by dissolving 10 g of PVA (SD fine Chemicals, $M_w = 14\,000$, degree of hydrolysis 98%) in 100 ml double distilled water at 90 °C for 4 h. Aminoclay solutions at different concentrations (2, 4, 6, 8, 10, and 20 wt % with respect to PVA) were exfoliated separately in 20 mL of distilled water by sonication for 5 min. The polymer–clay ratio was controlled by the stoichiometric addition of clay dispersion to a fixed quantity of PVA solution followed by stirring and sonicating for 5 min. The films were casted in polypropylene Petri dishes kept on a leveled surface. The films were allowed to dry slowly at room temperature for 2 days so that the irregularities caused during the evaporation of water will be minimized. The thickness of the film obtained was in the range of 75–100 μm. Nanoparticle-stabilized aminoclay–PVA nanocomposites were also prepared in a similar manner and used for characterization. PVA–montmorillonite (Cloisite Na^+, Southern Clay Products, TX) composites were also prepared for comparing mechanical properties.

Scheme 1. Flowchart Showing the Synthesis of Aminoclay, Aminoclay–PVA Nanocomposite Films, and Metal-Nanoparticle-Loaded Aminoclay–PVA Nanocomposite Films

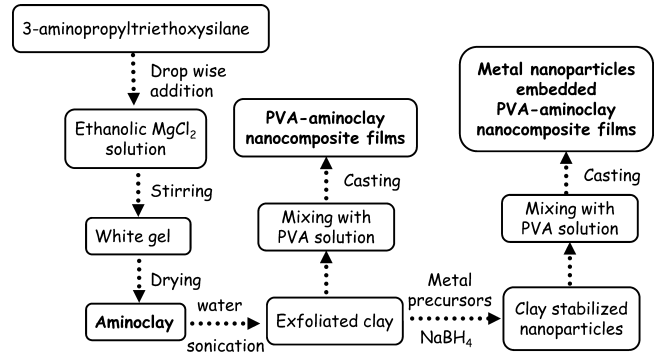

Characterization Techniques. Purity and structure of synthesized aminoclay, pure PVA, and PVA–aminoclay nanocomposites were analyzed by powder X-ray diffraction (XRD) patterns recorded using Bruker DS discover diffractometer (CuKα radiation, $\lambda = 1.54$ Å, θ scanning range 1–80°, Step size: 0.011, Current: 40 mA and Voltage: 40 KV). UV–vis absorption spectra of Ag and Au nanoparticles composite films were recorded by using Perkin Elmer UV/Vis/NIR spectrometer (Model: Lambda 900). The IR spectra of the self-supported composite films were recorded using Thermo Nicolet FTIR spectrometer (Model 5700, Madison, WI) fitted with single bounce attenuated total reflectance (ATR) accessory with ZnSe crystal. Sixty-four scans were averaged to reduce the noise and all spectra were recorded at 4 cm^{-1} resolution. Field-emission scanning electron microscopic (FESEM) images and energy-dispersive analysis of X rays (EDAX) were obtained by means of FEI (Nova-Nano SEM-600 Netherlands). All the images were taken at low vacuum using an operating voltage of 5 kV.

Mechanical and stress relaxation properties of nanocomposites films were determined in the tensile mode using Lloyd Instruments (model LRX Plus) UTM using a strain rate of 100 mm/min. Rectangular samples (5 in. × 1 in.) were prepared from the nanocomposite films as per ASTM D882. Relaxation of stress in PVA–nanocomposite films were continuously monitored by stretching them to 2% strain and holding them in that position for 90 min. An automatic manometric gas permeability tester (LYSSY AG, Model L100-5000) was used to measure the oxygen transmission rate through the nanocomposite films. Samples of the size 100 × 110 mm^2 were mounted between the test cells having a test area of 50 cm^2 in the center for determining the gas permeability at 23 °C. Differential Scanning Calorimetry (DSC) measurements of pure PVA and its nanocomposites were carried out using DSC 2010, TA Instruments in the temperature range of −30 °C to 225 °C under nitrogen atmosphere. Sealed pans with samples were first cooled to −30 °C, held isothermally for 1 min, and then ramped (10 °C / min) to 225 °C to obtain heat flow curves.

RESULTS AND DISCUSSIONS

The optical image of the polymer–nanocomposite films containing 10 wt % aminoclay shows the transparent nature of the hybrid films due to nanoscale dispersion of exfoliated clay layers (Figure 1A). The uniform distribution of pink and yellow color throughout the Au- and Ag-loaded composite film further indicates that the nanoparticles were spread evenly in the PVA matrix. The nanoparticles are first stabi-

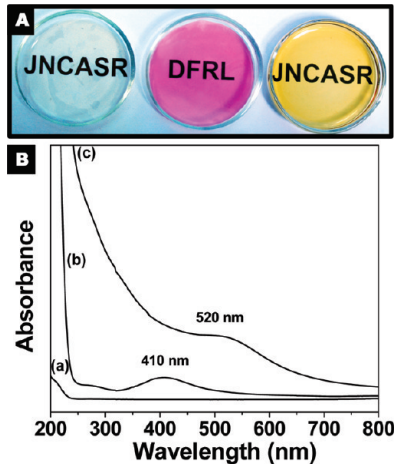

FIGURE 1. (A) Optical image of the nanocomposite films; from left to right, PVA−aminoclay, Au-nanoparticle-loaded PVA−aminoclay, and Ag-nanoparticle-loaded PVA−aminoclay. (B) UV−vis absorption spectra of (a) PVA−aminoclay, (b) Ag-nanoparticle-loaded PVA−aminoclay, and (c) Au-nanoparticle-loaded PVA−aminoclay.

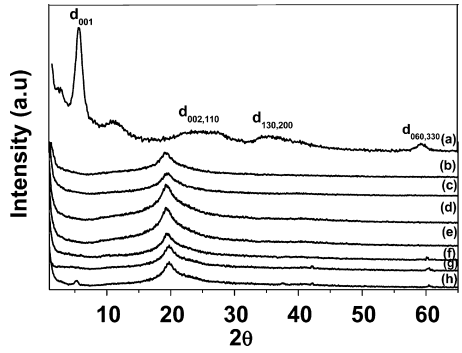

FIGURE 2. XRD patterns of (a) aminoclay, (b) pure PVA, and PVA−aminoclay nanocomposites with different proportions of aminoclay: (c) 2,(d) 4, (e) 6, (f) 8, (g) 10, and (h) 20 wt %.

lized with the aminoclay before being admixed with PVA. Because the Ag and Au nanoparticles interaction with the aminoclay is very strong and cannot be dislodged even by the alkane thiols (22), it is understood that the evenly spread plasmon color associated with the Ag and Au nanoparticles is an indirect measure of the homogeneous mixing of the aminoclay sheets within the PVA matrix. UV−vis absorption spectra (Figure 1B) for Ag and Au nanoparticles containing nanocomposite films show characteristic surface plasmon resonance bands at 410 and 520 nm, respectively.

Figure 2 shows the powder X-ray diffraction (PXRD) patterns of PVA-aminoclay nanocomposites at different loadings of the aminoclay. The as-synthesized aminoclay exhibits a basal distance (d_{001}) of 1.51 nm, along with broad in-plane diffraction peaks ($d_{020,110}$ = 0.414 nm and $d_{130,220}$ = 0.254 nm) respectively. The characteristic (d_{060}) diffraction peak around $2\theta = 60°$ corresponding to the 2:1 trioctahedral smectite clay is weak due to the staking disorder induced by the organofunctional groups.

On the other hand, PVA possess a broad d_{101} peak at $2\theta = 19°$, the characteristic peak of semi-crystalline polymers (23). The intensity of this peak more or less retained even at higher clay loading suggesting that the crystalline behavior of the polymer was not affected much by the introduction of aminoclay. The absence of d_{001} peak corresponding to the aminoclay in the nanocomposites even at higher loading confirms the extensive exfoliation of clay within the polymer. The emergence of a weak peak at higher d_{001} spacing (1.68 nm) for the 20 wt % clay loading suggests the existence of a very small amount of intercalated layered silicates in addition to the exfoliated form. The slight increase in d_{001} spacing from 1.51 nm appeared for the pure aminoclay to 1.68 nm for the PVA−clay composite confirms the intercalation of PVA chains within the intergalleries of aminoclay at higher loadings. FTIR spectrum of PVA aminoclay nanocomposites (see the Supporting Information, S-1) shows an additional band around 1510 cm^{-1}, which corresponds to the deformation of -NH_2 groups present in the aminoclay. The coexistence of this band along with other characteristic peaks of PVA confirms the presence of aminoclay in PVA.

Various properties of the clay−polymer nanocomposites are influenced by the morphological nature of the composites. For example, the mechanical and gas permeable properties of polymer−clay nanocomposites are highly related to their morphology. Several factors such as size and shape of the nanofiller, volume fraction of the nanofiller, clustering of the nanofiller, and nature of the polymer are reported to influence the morphology of the polymer−clay nanocomposites (24). The field emission scanning electron microscopic (FESEM) images of PVA−aminoclay nanocomposites at different aminoclay loadings shown in Figure 3 reveal the retention of nanomorphology of the aminoclay even at higher loading. The FESEM image of the nanocomposite containing 6 wt % aminoclay shows uniform distribution of clay nanoparticles throughout the film (Figure 3a). Regions where these clay nanoparticles begin to form network nanostructures by connecting with neighboring clay particles are also clearly seen from the image. As the clay loading increases to 8 wt % and above, a dendrite-like nanostructure networks developed for the dispersed clay over the polymer matrix (Figure 3b−d). The presence of silica and magnesium peaks in the EDAX spectrum (Figure 3b, inset) for these dendrite structures confirms the existence of clay in the PVA matrix. It appears that at higher loading the bulky stacked-sheet like morphology normally expected for the layered structures is disfavored in the case of aminoclay because of the fragmentation of large two-dimensional clay sheets into tiny slabs during exfoliation by sonication. The phase segregation and packing of these small clay nanoslabs at higher concentration lead to the formation of nanoscale dentritic pattern (Figure 3b), a significant deviation from sheetlike structure with the ligament size varied from 50 to 100 nm within the PVA matrix. The optical clarity obtained in the visible region (Figure 1A) also strengthens our FESEM observation that the organization of clay layers occurs only at the nanoscale even at higher amount of aminoclay loading. The absence of any low-angle d_{001} peak in the XRD pattern (Figure 2g) indicates that the staking of these aminoclay slabs are not that ordered at the nanoscale level. It is to be noted that the Ag or Au nanoparticles containing aminoclay−PVA nanocomposites did not show any distinct dendrite-like

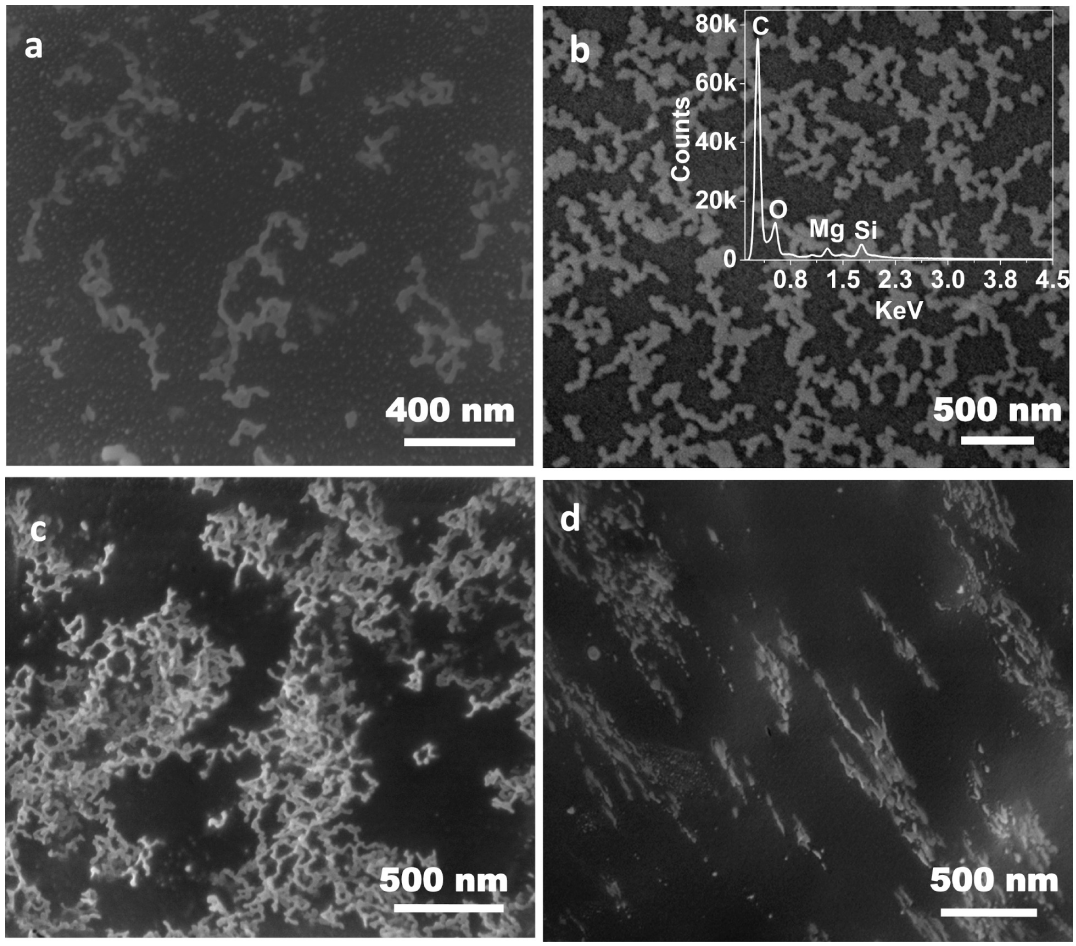

FIGURE 3. FESEM images of PVA−aminoclay nanocomposites (top view) containing various proportions of aminoclay (a) 6 (inset shows the corresponding EDAX spectra), (b) 8, (c) 10, and (d) 8 wt % (cross-sectional view).

network structures even though the clay nanoparticles are located very close to each other at 10 wt % loading (see the Supporting Information, S-2). This suggests that the anchored Ag nanoparticles on the aminoclay layers leave a roughened surface, which will not favor the network formation through staking of adjacent layers. Furthermore, the spreading of organic groups on the surface of the Ag or Au nanoparticles reduces the hydrophobic interactions between the organic layers, the driving force for the staking of layers while drying (Scheme 2).

The stress−strain behavior of pure PVA as well as PVA−aminoclay nanocomposites is shown in Figure 4A. The stress-strain curve for PVA−montmorillonite nanocomposites is also shown in Figure 4B for comparison. Pure PVA shows a behavior typical of plastic materials with significant yielding. PVA due to its large free volume and low glass-transition temperature cannot withstand high stresses in comparison to the inorganic phase with low free volume and high glass-transition temperature. Intimate mixing of these two phases likely to improve the mechanical strength of the resulting composite (25). A considerable improvement in the tensile strength is visible as the PVA is reinforced with aminoclay or montmorillonite. The tensile stress required for plastic yielding increases from 33 MPa for the pure PVA to 48 MPa (nearly 45 % increase) for the 20 wt % aminoclay loaded PVA composite. As expected, for an equal amount

Scheme 2. Schematic Showing the Dispersion of (a) Aminoclay Layers (10 wt %) within the PVA Matrix and (b) Ag-Nanoparticle-Stabilized Aminoclay Layers (10 wt %) within PVA Matrix; Nanoparticles Give Roughness to the Clay Particle Surface

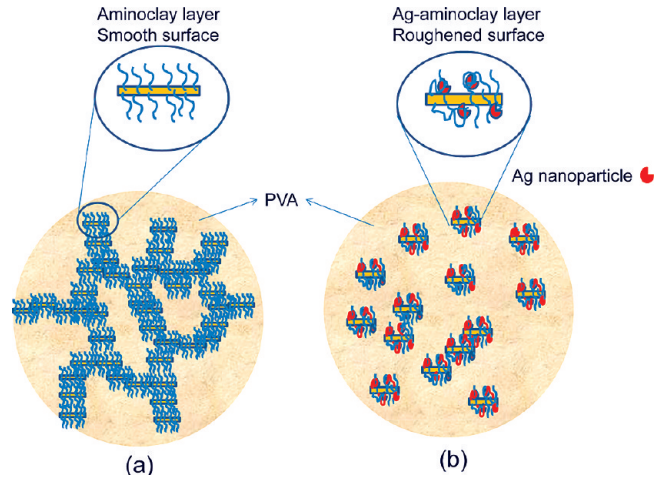

of clay loading, aminoclay−PVA nanocomposite shows relatively lower tensile stress at break because of the presence of organic propylamino groups compared to the montmorillonite-PVA composite. The main advantage of having aminoclay filler is that it is not imparting any additional

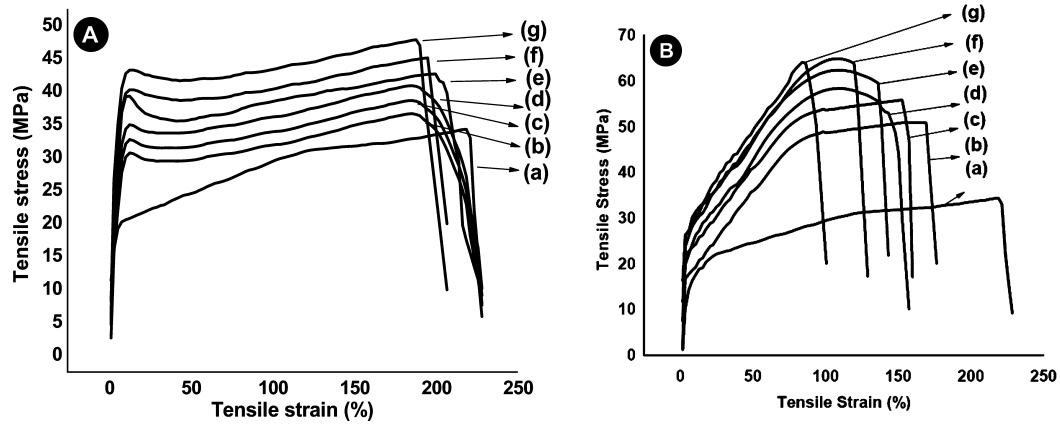

FIGURE 4. Stress strain curves of (A) (a) pure PVA and PVA−aminoclay nanocomposites; (B) (a) pure PVA and PVA− montmorillonite with different proportions of clays: (b) 2, (c) 4, (d) 6, (e) 8, (f) 10, and (g) 20 wt %.

brittleness to the PVA compared to montmorillonite clay particles (10). For example, the composite containing 20 wt % montmorillonite shows nearly 60% reduction in the tensile strain, whereas the aminoclay for the same weight percentage shows only 20% reduction in the plastic yielding before rupture. The increased brittleness in clay composites is usually attributed to the decreased miscibility between organic polymer and inorganic nanofillers. When organically modified montmorillonite clay is used as the filler, the composite becomes more and more brittle as the clay weight percentage increases and fails immediately after the initial elastic region, whereas when aminoclay was used as the filler, the resulting composite displays improved flexibility and strength as the clay content increases. Our tailormade aminoclay is designed to have covalently linked short-chain amino groups, in order to increase its miscibility in water and water-soluble polymers. Contrary to the montmorillonite−PVA composites, the interaction between clay nanoparticles and the polymer matrix in aminoclay−PVA nanocomposites is mediated by the propylamino groups, which would influence the particle behavior and its spatial distribution (2). Moreover, the amine groups are expected to improve the adhesion properties between inorganic matrix and polymer through hydrogen bonding (5). The interaction between hydroxyl groups of PVA and amino groups of clay can impart additional reinforcement to the polymer matrix and hence improve its mechanical properties considerably. Furthermore, the introduction of organic components between the inorganic platelets is known to arrest the crack propagation by dissipating the energy within the organic layers and hence improve the toughness of the materials (5, 18, 26, 27). Interestingly, aminoclay−PVA nanocomposite containing a small amount of Ag nanoparticles (Figure 5) shows a significant enhancement in its mechanical properties. Introduction of Ag nanoparticles (0.02 wt % Ag with respect to PVA−aminoclay nanocomposite) embedded aminoclay shows a considerable improvement in its tensile strength as well as tensile modulus even at a lower concentration of clay (2 wt %). A comparison of tensile modulus, percentage elongation at break and tensile strength values for PVA−clay nanocomposites and Ag nanoparticles loaded aminoclay−PVA nanocomposites is given

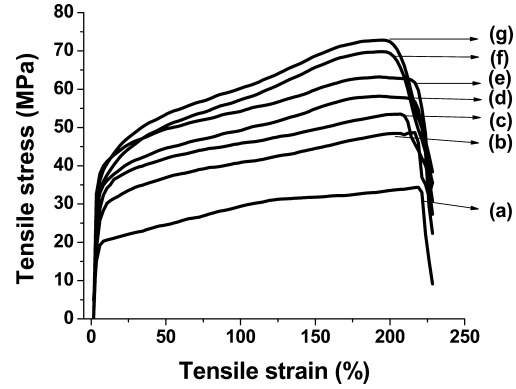

FIGURE 5. Stress strain curves of (a) pure PVA and PVA−aminoclay nanocomposites with different proportions of aminoclay embedded with Ag nanoparticles: (b) 2, (c) 4, (d) 6, (e) 8, (f) 10, and (g) 20 wt % nanocomposites.

in Table 1. From the table, it is observed that the elongation at break did not show any significant change for the nanocomposites irrespective of the aminoclay content in PVA. Even the metal nanoparticles loaded nanocomposites show higher value of elongation at break. However, the tensile modulus shows a different behavior for the PVA−aminoclay nanocomposites compared to the metal nanoparticles containing aminoclay−PVA nanocomposites. The tensile modulus of PVA gradually increases with increase in aminoclay loading. For example, it increases from 418 MPa for pure PVA to 855 MPa for the 20 wt % aminoclay loaded PVA, a 100 % increase compared to the pure PVA, although this increase is relatively low compared to the montmorillonite loaded PVA nanocomposites (10). On the other hand, Ag nanoparticles containing aminoclay−PVA nanocomposites almost attained a higher value (833 MPa) even for the 2 wt % aminoclay loading, signifying the important role played by the Ag nanoparticles in reinforcing the nanocomposites. Further addition of Ag nanoparticles containing aminoclay, however, did not show any marked increase in its tensile modulus (950 MPa for 20 wt % PVA−aminoclay nanocomposite).

The high surface to volume ratio of nanoparticles as well as the strong interfacial interaction of Ag nanoparticles with the aminoclay and PVA are responsible for the efficient transfer of load from the polymer to the high modulus

Table 1. Tensile strength, Elongation at Break, and Tensile Modulus of (A) Pure PVA, (B) aminoclay–PVA Nanocomposites, and (C) Ag-Nanoparticle-Containing Aminoclay–PVA Nanocomposite at Different Clay Loading

sample	clay content (wt %)	tensile strength (MPa)	elongation at break (%)	tensile modulus (MPa)
A	Nil	28 ± 3.2	223 ± 28.5	418 ± 53.9
B	2	36 ± 3.5	183 ± 25.7	586 ± 51.7
	4	38 ± 3.1	185 ± 23.7	614 ± 57.9
	6	39 ± 4.0	186 ± 27.6	685 ± 60.7
	8	43 ± 4.5	214 ± 25.9	736 ± 63.1
	10	45 ± 4.2	200 ± 23.6	792 ± 61.2
	20	48 ± 4.1	188 ± 18.4	855 ± 60.6
C	2	48 ± 3.9	221 ± 27.9	833 ± 64.5
	4	53 ± 5.0	218 ± 30.5	889 ± 71.8
	6	58 ± 4.7	228 ± 24.0	897 ± 66.8
	8	63 ± 5.4	229 ± 28.4	912 ± 68.6
	10	69 ± 5.6	216 ± 23.7	953 ± 69.3
	20	72 ± 5.1	214 ± 25.4	950 ± 65.4

inorganic fillers and hence improve the tensile stress needed for the plastic yielding (28). Additionally, a strain-hardening region is also visible at the end of necking region, which is not prominent in the case of aminoclay alone incorporated PVA nanocomposites. This may be due to the additional reinforcement provided by Ag and Au nanoparticles. These results indicate that Ag and Au nanoparticles are significantly contributing to the enhanced mechanical properties of these nanocomposites.

Figure 6 shows the stress relaxation curve for PVA and its nanocomposites, normalized with respect to initial stress. Inset shows the corresponding stress relaxation of nanocomposites having Ag nanoparticles. The decrease in residual stress with time suggests the reduced stability of pure polymers PVA on prolonged loading. Though a gradual improvement in stress relaxation is observed with the increased loading of aminoclay in the PVA matrix, the stress–relaxation behavior more or less followed the same path as pure PVA. Whereas, the addition of presynthesized Ag nanoparticles that are stabilized by aminoclay considerably enhances the stress relaxation properties of the composites with a notable arrest in the decrease in residual stress at the initial period itself (Figure 6, inset). This suggests that the nanoparticles that are known to affect the polymer viscoelastic properties can prevent the cold flow, which in turn reduces the stress relaxation (28).

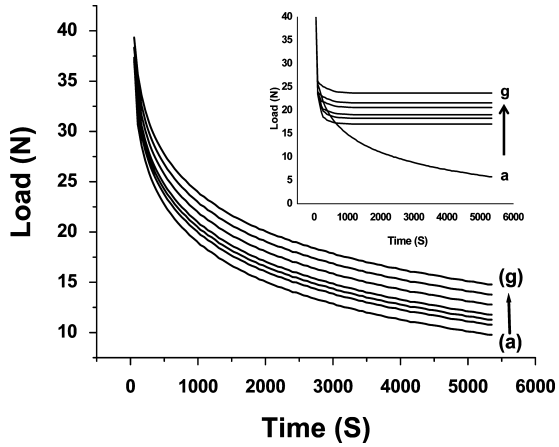

FIGURE 6. Stress relaxation curves of (a) pure PVA and PVA–aminoclay nanocomposites with different proportions of aminoclay (b) 2, (c) 4, (d) 6, (e) 8, (f) 10, and (g) 20 wt %. Inset shows the corresponding stress relaxation curve of PVA aminoclay nanocomposites embedded with 0.02 wt % (wrt PVA–clay nanocomposite) silver nanoparticles.

The glass-transition temperature, T_g of the polymer nanocomposites strongly influenced by the extent of interaction between nanoparticles and the polymer chains, particle dispersion and the interparticles spacing (29). If the interaction between particles and the polymer chain is too weak, the nanocomposite is reported to show lower T_g value than the bulk polymer T_g (1, 30). If the interaction is too strong, the nanocomposites are shown to exhibit two T_g values, one for the polymer chain away from the nanoparticles and the other for the polymer chain interacting with the nanoparticles (31). The T_g associated with the latter is usually larger than the bulk polymer T_g due to slower relaxation dynamics of the polymer chain near the nanoparticles (32). If the interaction is not too strong and there is no permanent attachment of polymer chain to the nanoparticles, the nanocomposite would show single but larger T_g due to longer relaxation time. The single, yet slightly larger T_g values obtained for all our PVA-aminoclay nanocomposites (Table 2 and the Supporting Information, S-3) suggest that the enthalpic interaction between aminoclay and the PVA polymer is not too strong, although the mixing between the clay and the polymer is very good. Furthermore, the observation of both T_g and T_m in DSC for the aminoclay–PVA nanocomposites at all compositions did not support the nanoconfinement of PVA chains within the aminoclay layers. Nanoconfinement in the neatly intercalated PVA–MMT nanocomposites resulted in the disappearance T_g and the melting temperature, T_m of the PVA (10). The absence of any noticeable low angle peak in the XRD pattern (Figure 2) for the aminoclay–PVA nanocomposites also confirms the complete exfoliation and mixing of aminoclay layers with the polymer chain rather than confining the PVA within the galleries. Because of the intimate mixing of aminoclay with the PVA chains at the nanolevel, all the polymer is equally affected or to some extent immobilized by the clay compo-

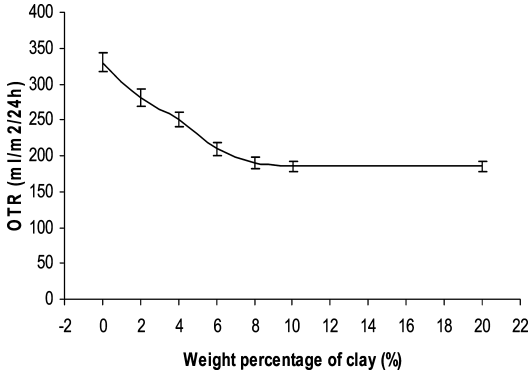

FIGURE 7. Oxygen transmission rates of PVA aminoclay nanocomposite films.

Table 2. Glass-Transition Temperatures, T_g, Values of Pure PVA, PVA−Aminoclay, PVA−Montmorillonite Clay, and Ag-Nanoparticle-Embedded Aminoclay−PVA Nanocomposites

sample	T_g (°C)
PVA	36.3
PVA + 2% aminoclay	41.6
PVA + 4% aminoclay	42.9
PVA + 6% aminoclay	42.7
PVA + 8% aminoclay	43.3
PVA + 10% aminoclay	44.1
PVA + 20% aminoclay	45.0
PVA + 20% montmorillonite	44.9
PVA + 2% aminoclay with Ag nanoparticles	47.1
PVA + 4% aminoclay with Ag nanoparticles	47.4
PVA + 6% aminoclay with Ag nanoparticles	45.4
PVA + 8% aminoclay with Ag nanoparticles	38.9
PVA + 10% aminoclay with Ag nanoparticles	37.8
PVA + 20% aminoclay with Ag nanoparticles	39.8

nent and therefore shows only one T_g value, which is higher than the T_g of bulk polymer, 36.28 °C (Table 2). The presence of small amount of Ag nanoparticles also show a single, but higher T_g (47.13 °C) value for 2 wt % aminoclay loading, which was higher than the value obtained for 20 wt % aminoclay loading(T_g = 45.01°C) without Ag nanoparticles. In addition, these nanocomposites show a significant reduction in the melting temperature, T_m (about 10−15 °C reduction in T_m), compared to the T_m value of pure PVA (around 200 °C, see the Supporting Information, S-3), probably because of the existence of PVA in a different crystalline phase than the bulk polymer phase (10, 23).

The barrier properties like oxygen transmission rate (OTR) of PVA nanocomposite films have been summarized in Figure 7. The incorporation of aminoclay reduced OTR considerably, which can be explained by considering the layered clay sheets as impermeable obstacles in the path of oxygen diffusion process. In a well-exfoliated state, individual clay platelets create a tortuous path that reduces the transmission of gas and vapor molecules through the PVA matrix. As the clay concentration increased beyond 10 wt % in PVA, the reduction in OTR is marginal, probably because of the phase segregation.

CONCLUSIONS

Water-dispersible nanoclays having hydrophilic pendant organic groups were synthesized and used for fabricating PVA nanocomposite films having excellent transparency and flexibility. The mechanical property of PVA was improved significantly by the introduction of metal nanoparticles anchored aminoclay. The addition of Ag nanoparticles considerably enhanced the stress relaxation properties of these nanocomposites. Oxygen transmission rate of these nanocomposites decreased as clay platelets created a tortuous path for the incoming gaseous molecules. Synthesizing nanocomposites having different nanoparticles existing together is a simple and efficient method to integrate and improve desired properties without compromising much of the inherent properties of PVA. These materials will have a lot of potential applications especially in the food packaging area, where smart packaging materials having excellent mechanical, ductile, and barrier properties along with antimicrobial properties are required to cater the future needs of both military and civilian applications.

Acknowledgment. The authors thank Prof. C. N. R. Rao, FRS, for his kind support and encouragement. G.J. thanks the Jawaharlal Nehru Centre for Advanced Scientific Research for its Visiting Fellowship Program.

Supporting Information Available: FTIR spectra of pure PVA and its aminoclay nanocomposites, FESEM images of PVA−Ag−aminoclay and PVA−Au−aminoclay nanocomposites and DSC curves of pure PVA and its aminoclay nanocomposites (PDF). This material is available free of charge via the Internet at http://pubs.acs.org.

REFERENCES AND NOTES

(1) Oh, H.; Green, P. F. *Nat. Mater.* **2009**, *8*, 139–143.
(2) Balazs, A. C.; Emrick, T.; Russell, T. P. *Science.* **2006**, *314*, 1107–1110.
(3) Vaia, R. A.; Jandt, K. D.; Kramer, E. J.; Giannelis, E. P. *Chem. Mater.* **1996**, *8*, 2628–2635.
(4) Kumar, S. A.; Yuelong, H.; Yumei, D.; Le, Y.; Kumaran, M.G.; Thomas, S. *Ind. Eng. Chem. Res.* **2008**, *47*, 4898–4904.
(5) Bonderer, L.J.; Studart, A. R.; Gauckler, L. J. *Science.* **2008**, *319*, 1069–1073.
(6) Lan, T.; Kaviratna, P. D.; Pinnavaia, T. J. *Chem. Mater.* **1994**, *6*, 573–575.
(7) Tyan, H-L; Liu, Y.-C.; Wei, K.-H. *Chem. Mater.* **1999**, *11*, 1942–1947.
(8) Wang, Z.; Pinnavaia, T. J. *Chem. Mater.* **1998**, *10*, 3769–3771.
(9) Sun, T.; Garcés, J. M. *Adv. Mater.* **2002**, *14*, 128–130.
(10) Strawhecker, K. E.; Manias, E. *Chem. Mater.* **2000**, *12*, 2943–2949.
(11) Vaia, R. A.; Sauer, B. B.; Tse, O. K.; Giannelis, E. P. *J Polym Sci., Part B: Polym Phys* **1997**, *35*, 59–67.
(12) Krikorian, V.; Pochan, D. J. *Chem. Mater.* **2003**, *15*, 4317–4324.
(13) Muthuswamy, E.; Walsh, D.; Mann, S. *Adv. Mater.* **2002**, *14*, 969–972.
(14) Burkett, S. L.; Press, A.; Mann, S. *Chem. Mater.* **1997**, *9*, 1071–1073.
(15) Lebeau, B.; Brendle, J.; Marichal, C.; Patil, A. J.; Muthuswamy, E.; Mann, S. *J Nanosci. Nanotechnol.* **2006**, *6*, 352–359.
(16) Bassner, S. L.; Klingenberg, E. H. *Am. Ceram. Soc. Bull.* **1998**, *77*, 71–75.
(17) Podsiadlo, P.; Kaushik, A. K.; Shim, B. S.; Agarwal, A.; Tang, Z.; Waas, A. M.; Arruda, E. M.; Kotov, N. A *J. Phys. Chem. B.* **2008**, *112*, 14359–14363.
(18) Podsiadlo, P.; Kaushik, A. K.; Arruda, E. M.; Waas, A. M.; Shim, B. S.; Xu, J.; Nandivada, H.; Pumplin, B. G.; Lahann, J.; Ramamurthy, A.; Kotov, N. A. *Science* **2007**, *318*, 80–83.

(19) Wypych, F.; Satyanarayana, K. G. *J. Colloid Interface Sci.* **2005**, *285*, 532–543.
(20) Datta, K. K. R.; Srinivasan, B.; Balaram, H.; Eswaramoorthy, M. *J. Chem. Sci.* **2008**, *120*, 579–586.
(21) Patil, A. J.; Muthuswamy, E.; Mann, S. *Angew. Chem., Int. Ed.* **2004**, *43*, 4928–4933.
(22) Datta, K. K. R.; Eswaramoorthy, M.; Rao, C. N. R. *J. Mater. Chem.* **2007**, *17*, 613–615.
(23) Yu, Y.-H.; Lin, C.-Y.; Yeh, J.-M.; Lin, W.-H. *Polymer.* **2003**, *44*, 3553–3560.
(24) Zenga, Q.H.; Yua, A.B.; Lu, G.Q. *Prog. Polym. Sci.* **2008**, *33*, 191–269.
(25) Zulfiqar, S.; Kausar, A.; Rizwan, M.; Sarwar, M. I. *Applied Surface Science.* **2008**, *255*, 2080–2086.
(26) Mann, S *Biomineralization: Principles and Concepts in Bioinorganic Materials Chemistry*; Oxford University Press: Oxford, U.K., 2001.
(27) Priestley, R. D.; Ellison, C. J.; Broadbelt, L. J.; Torkelson, J. M. *Science.* **2005**, *309*, 456–459.
(28) Mbhele, Z. H.; Salemane, M. G.; van Sittert, C. G. C. E.; Nedeljkovic, J. M.; Djokovic, V.; Luyt, A. S. *Chem. Mater.* **2003**, *15*, 5019–5024.
(29) Kropka, J. M.; Putz, K. W.; Pryamitsyn, V.; Ganesan, V.; Green, P. F. *Macromolecules* **2007**, *40*, 5424–5432.
(30) Bansal, A.; Yang, H.; Li, C.; Cho, K.; Benicewicz, B. C.; Kumar, S. K.; Schadler, L. S. *Nat. Mater.* **2005**, *4*, 693–698.
(31) Tsagaropoulos, G.; Eisenber, A. *Macromolecules* **1996**, *28*, 396–398.
(32) Starr, F. W.; Schrøder, T. B.; Glotzer, S. C. *Macromolecules* **2002**, *35*, 4481–4492.

AM9005226